

Modeling of matter-wave solitons in a nonlinear inductor-capacitor network through a Gross-Pitaevskii equation with time-dependent linear potential

E. Kengne,¹ A. Lakhssassi,¹ and W. M. Liu²¹*Département d'informatique et d'ingénierie, Université du Québec en Outaouais, 101 Rue Saint-Jean-Bosco, Succursale Hull, Gatineau (PQ), Canada J8Y 3G5*²*Institute of Physics, Chinese Academy of Sciences, No. 8 South-Three Street, ZhongGuanCun, Beijing 100190, China*

(Received 24 June 2017; revised manuscript received 11 August 2017; published 29 August 2017)

A lossless nonlinear LC transmission network is considered. With the use of the reductive perturbation method in the semidiscrete limit, we show that the dynamics of matter-wave solitons in the network can be modeled by a one-dimensional Gross-Pitaevskii (GP) equation with a time-dependent linear potential in the presence of a chemical potential. An explicit expression for the growth rate of a purely growing modulational instability (MI) is presented and analyzed. We find that the potential parameter of the GP equation of the system does not affect the different regions of the MI. Neglecting the chemical potential in the GP equation, we derive exact analytical solutions which describe the propagation of both bright and dark solitary waves on continuous-wave (cw) backgrounds. Using the found exact analytical solutions of the GP equation, we investigate numerically the transmission of both bright and dark solitary voltage signals in the network. Our numerical studies show that the amplitude of a bright solitary voltage signal and the depth of a dark solitary voltage signal as well as their width, their motion, and their behavior depend on (i) the propagation frequencies, (ii) the potential parameter, and (iii) the amplitude of the cw background. The GP equation derived in this paper with a time-dependent linear potential opens up different ideas that may be of considerable theoretical interest for the management of matter-wave solitons in nonlinear LC transmission networks.

DOI: [10.1103/PhysRevE.96.022221](https://doi.org/10.1103/PhysRevE.96.022221)

I. INTRODUCTION

For many decades, the formation and propagation of nonlinear matter waves in nonlinear dispersive media have been the subjects of intensive studies [1–12]. Many studies show that nonlinear electrical networks (NLENWs) appear as a good example of real nonlinear dispersive media that allows one to study the different properties of solitary waves and to model the exotic properties of new systems [3,5,12–21].

A NLENW comprises a transmission line periodically loaded with varactors, where capacitance nonlinearity arises from a variable depletion layer width, which depends both on the dc bias voltage and on the ac voltage of the propagating wave. For example, the model shown in Fig. 1 [22] is a one-dimensional (1D) discrete electrical network made of ladder-type LC circuits containing constant inductors, voltage-dependent capacitors, and dissipative elements [16,18,22]. The nonlinear capacitors are usually reverse-biased capacitance diodes.

As far we know, work on the dynamics of matter-wave solitons in Noguchi electrical networks based on the Gross-Pitaevskii (GP) equation are lacking. In this paper, we aim to apply the reductive perturbation method in the semidiscrete limit [6] to show that the dynamics of modulated waves in a modified lossless Noguchi electrical network shown in Fig. 1 can be governed by a Gross-Pitaevskii equation with a linear potential. We investigate the modulational instability of our system and derive the analytical expression for the growth rate (gain) in terms of the coefficients of the derived GP equation. Then, we derive some analytical solitary wave solutions of the derived GP equation of the dynamics. Obtaining such analytical solutions allows one to test the validity of the Gross-Pitaevskii equation, obtain the long-time evolution of the soliton where numerical techniques may fail, and helps to

understand soliton formation and propagation in the network. The outline of the paper is as follows. In Sec. II, we present our model, derive a Gross-Pitaevskii equation with a linear potential that describes the dynamics of modulated waves in the networks, and investigate the modulational instability (MI) of the continuous-wave solution of the derived GP equation. Through exact solitonic solutions of the GP equation of the dynamics, we investigate analytically the soliton propagation in our model in Sec. III. Section IV concludes our paper.

II. MODEL DESCRIPTION AND GP EQUATION OF THE DYNAMICS

A. Model description and basic equations

The model used in this paper is the modified Noguchi one-dimensional (1D) electrical network illustrated in Fig. 1. The nonlinear capacitor C of the network consists of a reverse-biased diode with differential capacitance functions of the voltage V_n across the n th capacitor. This capacitor is biased by a constant voltage V_b and depends on the voltage V_n , for low voltage, at cell n as $C(V_b + V_n) = \frac{dQ_n}{dt} \approx C_0(1 - 2\alpha V_n + 3\beta V_n^2)$, where $C_0 = C(V_b)$ is the characteristic capacitance, α and β are the nonlinear coefficients of the electrical stored charge Q_n , and n is for the number of cells in the network [3,22,23].

Applying Kirchhoff's laws on the network of Fig. 1 yields a system of nonlinear discrete equations

$$\begin{aligned} \frac{d^2 V_n}{dt^2} + u_0^2(2V_n - V_{n-1} - V_{n+1}) + \omega_0^2 V_n + \frac{G_2}{C_0} \frac{dV_n}{dt} \\ + \lambda_S \frac{d^2}{dt^2}(2V_n - V_{n-1} - V_{n+1}) \\ = \frac{d^2}{dt^2}(\alpha V_n^2 - \beta V_n^3), \quad n = 1, 2, \dots, N, \end{aligned} \quad (1)$$

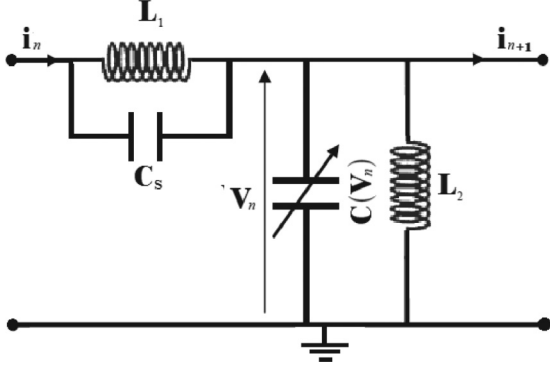


FIG. 1. Schematic representation of one unit cell of a dissipative modified discrete Noguchi electrical network with the linear inductor L_1 in parallel with a linear capacitance C_S in a series branch and a linear inductor L_2 in parallel with a nonlinear capacitor C in a parallel branch. The network is composed of N identical cells.

where $u_0 = \sqrt{(L_1 C_0)^{-1}}$ and $\omega_0 = \sqrt{(L_2 C_0)^{-1}}$ are the characteristic frequencies of the network, and $\lambda_s = C_S / C_0$. When using Eq. (1) to experience the transmission of matter-wave solitons through the model shown in Fig. 1, one excites the left extremity of the line and chooses the total number N of cells of the network so as not to encounter the wave reflection at the end of the network. In the numerical simulations, we will use the following typical line parameters [22],

$$\begin{aligned} L_1 &= 220 \mu\text{H}, & L_2 &= 470 \mu\text{H}, \\ V_b &= 2 \text{ V}, & C_0 &= C(V_b) = 370 \text{ pF}, \\ C_S &= 56 \text{ pF}, & \alpha &= 0.21 \text{ V}^{-1}, & \beta &= 0.0197 \text{ V}^{-2}. \end{aligned} \quad (2)$$

B. Gross-Pitaevskii equation of the dynamics

In this paper, we focus on waves with a slowly varying envelope in time and space with regard to a given angular frequency $\omega = \omega_p = 2\pi f_p$ and wave number $k = k_p$. In order to apply the reductive perturbation method [6, 18] to obtain short-wavelength envelope solitons, we introduce the slow envelope spatial and temporal variables $x = \varepsilon(n - v_g t)$ and $\tau = \varepsilon^2 t$, where ε is a small parameter that measures the smallness of the modulation frequency and the amplitude of the input waves, n is the cell number, and v_g is the group velocity of the linear wave packets. Therefore, voltage $V_n(t)$ of cell n at time t depends explicitly on the slow envelope variables x and τ so that we will be able to separate fast and slow variations of V_n in both space and time. The solution of (1) is then sought in the following general form [6],

$$\begin{aligned} V_n(t) &= \varepsilon u(x, \tau) \exp[i\theta] + \varepsilon^2 \psi_1(x, \tau) \\ &\quad + \varepsilon^2 \psi_2(x, \tau) \exp[2i\theta] + \text{c.c.}, \end{aligned} \quad (3)$$

where $\theta = kn - \omega t$ is the rapidly varying phase (k and ω are respectively the wave number and the angular frequency), and c.c. stands for the complex conjugation. The ε^2 terms, that is, the dc term $\psi_1(x, \tau)$ and the second-harmonic term $\psi_2(x, \tau)$, are added to the fundamental term $u(x, \tau)$ in order to take into account the asymmetry of the charge-voltage relation given by Eq. (1). During the computations, nonzero voltages $V_{n\pm 1}(t)$ lead to functions of the form $F(x \pm \varepsilon, \tau)$, which will

be expanded in the continuum limit around $F(x, \tau)$, that is, $F(x \pm \varepsilon, \tau) \approx F(x, \tau) \pm \varepsilon \frac{\partial F}{\partial x} + \frac{\varepsilon^2}{2} \frac{\partial^2 F}{\partial x^2} + \dots$, so that the fast changes of the phase θ in Eq. (3) are correctly taken into account by considering differences in the phase for the discrete variable n . Then we keep up to second order the derivative terms of F to balance dispersion and nonlinearity. Substituting Eq. (3) into Eq. (1) yields a series of inhomogeneous equations at a different order (ε , $\exp[i\theta]$).

The terms of $O(\varepsilon)$ for the first harmonic, that is, the equation at order (ε , $\exp[i\theta]$), leads to the linear dispersion relation of a typical passband filter,

$$\omega^2 = \frac{\omega_0^2 + 4u_0^2 \sin^2 \frac{k}{2}}{1 + 4\lambda_s \sin^2 \frac{k}{2}}, \quad (4)$$

in which the wave number k is taken in the Brillouin zone ($0 \leq k \leq \pi$). It is clear that the linear spectrum corresponding to the linear dispersion law (4) has a gap $f_0 = \omega_0/2\pi$ (corresponding to $k = 0$), which is the lower cutoff frequency introduced by the parallel inductance L_2 and is limited by the cutoff frequency $f_{\max} = \sqrt{(\omega_0^2 + 4u_0^2)/(1 + 4\lambda_s)}/2\pi$ due to the intrinsic discrete character of the lattice.

An equation at order (ε^2 , $\exp[i\theta]$) leads to the equation

$$\frac{\partial u}{\partial \tau} + \frac{d\omega}{dk} \frac{\partial u}{\partial x} = 0. \quad (5)$$

Equation (5) means that $u(x, \tau)$ represents a traveling wave moving with group velocity,

$$\begin{aligned} v_g &= \frac{d\omega}{dk} = \frac{(u_0^2 - \lambda_s \omega^2) \sin k}{\omega(1 + 4\lambda_s \sin^2 \frac{k}{2})} \\ &= \frac{(\frac{L_2}{L_1} C_0 - C_S) \sin k}{L_2 C_0 \omega (C_0 + 4C_S \sin^2 \frac{k}{2})^2}. \end{aligned}$$

For v_g to be non-negative in the Brillouin zone ($0 \leq k \leq \pi$), the linear capacitance C_S must satisfy the condition $C_S \leq L_2 C_0 / L_1$. At the limit $C_S = L_2 C_0 / L_1$, the group velocity v_g will be zero and the packets will not move (standing wave packets). When $C_S \rightarrow L_2 C_0 / L_1 - 0$, the group velocity v_g becomes nearly zero. It is important to notice that group velocities associated with the cutoff frequencies f_0 and f_{\max} are also zero. Therefore, wave packets with cutoff frequencies are standing waves.

An equation at order (ε^4 , $\exp[0i\theta]$) leads to the equation

$$\frac{\partial^2 \psi_1}{\partial x^2} = \frac{2\alpha\omega v_g^2}{v_g^2 - u_0^2} \frac{\partial^2 |u|^2}{\partial x^2},$$

with the general solution

$$\psi_1(x, \tau) = \frac{2\alpha\omega v_g^2}{v_g^2 - u_0^2} |u|^2 + \chi_0(\tau)x + \chi_1(\tau), \quad (6a)$$

where $\chi_0(\tau)$ and $\chi_1(\tau)$ are two arbitrary real functions of time τ . In the limit of standing waves, that is, when $C_S = L_2 C_0 / L_1$, Eq. (6a) leads to $\psi_1(x, \tau) = \chi_0(\tau)x + \chi_1(\tau)$.

At order (ε^2 , $\exp[2i\theta]$), we obtain the second-harmonic term $\psi_2(x, \tau)$ in terms of the fundamental term $u(x, \tau)$ as

$$\psi_2(x, \tau) = \frac{4\alpha\omega^2}{4\omega^2 - \omega_0^2 + 4(4\lambda_s \omega^2 - u_0^2) \sin^2 k} u^2. \quad (6b)$$

With the use of Eqs. (6a) and (6b), we obtain at order (ε^3 , $\exp[i\theta]$) the following equation,

$$i \frac{\partial \psi}{\partial \tau} + P \frac{\partial^2 \psi}{\partial x^2} + Q |\psi|^2 \psi + \lambda(\tau) x \psi = 0, \quad (7a)$$

where

$$\begin{aligned} \psi(x, \tau) &= u e^{-i \int \chi(\tau) d\tau}, \quad \lambda(\tau) = -\frac{\alpha \omega}{1 + 4\lambda_s \sin^2 \frac{k}{2}} \chi_0(\tau), \\ \chi(\tau) &= -\frac{\alpha \omega}{1 + 4\lambda_s \sin^2 \frac{k}{2}} \chi_1(\tau), \\ P &= -\frac{v_g^2}{2\omega} \left(1 + 4\lambda_s \sin^2 \frac{k}{2} \right) \\ &\quad + \left(\frac{u_0^2}{2\omega} - \frac{\lambda_s \omega}{2} \right) \cos k - 2\lambda_s v_g \sin k, \\ Q &= \omega \left(\frac{3\beta}{2} - \frac{4\alpha^2 \omega^2}{4\omega^2 - \omega_0^2 + 4(4\lambda_s \omega^2 - u_0^2) \sin^2 k} \right. \\ &\quad \left. - \frac{2\alpha^2 v_g^2}{v_g^2 - u_0^2} \right). \end{aligned} \quad (7b)$$

When $\lambda(\tau) = 0$, Eq. (7a) coincides with the nonlinear Schrödinger equation obtained in Ref. [22] when the dissipative term is ignored. Henceforth, we focus on the case when $\lambda(\tau)$ is not a trivial function. Equation (7a) under the condition $\lambda(\tau) \neq 0$ is known as a Gross-Pitaevskii equation with a linear potential [24,25]. In the context of Bose-Einstein condensates, $\psi(x, \tau)$ is the macroscopic wave function of the condensate, x is the coordinate normal to the surface of the condensate such that the bulk of the condensate exists in the region $x < 0$, and $V(x, \tau) = \lambda(\tau)x$ is the background or linear trapping potential and may correspond to the gravitational field with strength $\lambda(\tau)$. Also, $\chi(\tau)$ appearing in Eq. (7b) corresponds to the chemical potential of the system. In the absence of an external potential (i.e., $\lambda = 0$), Eq. (7a) becomes exactly integrable and supports both bright ($PQ > 0$) and dark ($PQ < 0$) solitary wave solutions. In the numerical calculations below, we will, for simplicity, work with $\chi_1(\tau) = 0$ so that $\psi(x, \tau) = u(x, \tau)$.

C. Modulational instability investigations in Noguchi electrical network

Equation (7a) admits the continuous-wave (cw) solution

$$\psi_c(x, \tau) = A_c \exp[i \Delta_c(x, \tau)], \quad (8a)$$

in which A_c is the constant real amplitude, $\Delta_c(x, \tau) = K_c(\tau)x + Q A_c^2 \tau - P \omega_c(\tau) + \delta_{0c}$ is the phase, and $K_c(\tau)$ and $\omega_c(\tau)$ are respectively the wave number and frequency of the carrier, satisfying the equations

$$\frac{dK_c}{d\tau} = \lambda(\tau), \quad \frac{d\omega_c}{d\tau} = K_c^2. \quad (8b)$$

To investigate the modulational instability of the carrier, we consider a small perturbation of the continuous-wave solution (8a) as follows,

$$\psi(x, \tau) = [1 + \delta\psi(x, \tau)] A_c \exp[i \Delta_c(x, \tau)], \quad (8c)$$

where $\delta\psi(x, \tau)$ is a small perturbation on the wave amplitude. Substituting Eq. (8c) into Eq. (7a) and keeping only linear terms in $\delta\psi$ and its complex conjugate yields

$$i \frac{\partial \delta\psi}{\partial \tau} + P \frac{\partial^2 \delta\psi}{\partial x^2} + 2i P K_c \frac{\partial \delta\psi}{\partial x} + Q A_c^2 [\delta\psi + \delta\psi^*] = 0. \quad (8d)$$

Now, we seek a solution for Eq. (8d) in the form

$$\begin{aligned} \delta\psi(x, \tau) &= B_1 \exp \left[i \left(Kx - \int_0^\tau \Omega(y) dy \right) \right] \\ &\quad + B_2^* \exp \left[-i \left(Kx - \int_0^\tau \Omega^*(y) dy \right) \right], \end{aligned} \quad (9)$$

where $Kx - \int_0^\tau \Omega(y) dy$ is the modulation phase, K and Ω are respectively the wave number and complex frequency of the modulation waves, and B_1 and B_2 two complex constants satisfying the condition $|B_1| + |B_2| > 0$. Inserting Eq. (9) into Eq. (8d) leads to the following homogeneous algebraic system with respect to B_1 and B_2 ,

$$[\Omega + Q A_c^2 - P K^2 - 2P K_c K] B_1 + Q A_c^2 B_2 = 0, \quad (10a)$$

$$-Q A_c^2 B_1 + [\Omega - Q A_c^2 - 2P K_c K + P K^2] B_2 = 0. \quad (10b)$$

For system (10a) and (10b) to admit nontrivial solutions, it is necessary and sufficient that its determinant should be zero:

$$(\Omega - 2P K_c K)^2 - K^2 P^2 (K^2 - 2P^{-1} Q A_c^2) = 0. \quad (10c)$$

Solving Eq. (10c) in Ω yields

$$\Omega(\tau) = 2P K_c K(\tau) \pm |P| K \sqrt{K^2 - 2P^{-1} Q A_c^2}, \quad (10d)$$

with $K_c = K_c(\tau)$ being any solution of the first equation in Eq. (8b). It follows from Eq. (10d) that for negative PQ , the frequency of modulation $\Omega(\tau)$ will be real for all wave numbers K , and the plane wave (8a) will be stable under modulation. For positive PQ , $\Omega(\tau)$ remains non-negative for wave number K satisfying the condition $K^2 \geq 2P^{-1} Q A_c^2$, leading to the modulational stability of the plane wave (8a). For wave numbers K satisfying the condition $0 < K^2 < 2P^{-1} Q A_c^2$, $\Omega(\tau)$ will have non-nil imaginary part for positive PQ , leading to the growth rate (gain) of modulational instability

$$|\text{Im}[\Omega(\tau)]| = |P| K \sqrt{2P^{-1} Q A_c^2 - K^2}. \quad (11)$$

In Eq. (11) the potential parameter $\lambda(\tau)$ defined by Eq. (7b) does not affect the domain of the MI of the continuous plane wave (8a). We have thus shown that the modulational (in)stability of the continuous plane wave solution (8a) of the GP Eq. (7a) with a linear potential only depends on the sign of the product PQ . With the use of the network parameters (2), we show in Fig. 2(a) the evolutions of the dispersive coefficient P (solid line) and nonlinear coefficient Q (dotted-dashed line) as functions of the wave number k of the carrier (dashed line). As we can see from the plot of P , the dispersive coefficient P is null for $k = k_z$, while the nonlinear coefficient Q is null for two values of k , k_{q1} and k_{q2} . From the plots of P and Q , it is seen that the product PQ is positive for $k \in]k_{q1}, k_z[\cup]k_{q2}, \pi[$, and negative for $k \in]0, k_{q1}[\cup]k_z, k_{q2}[$. Figure 2(b) shows the evolution of the frequency $f = \omega/2\pi$ as a function of wave

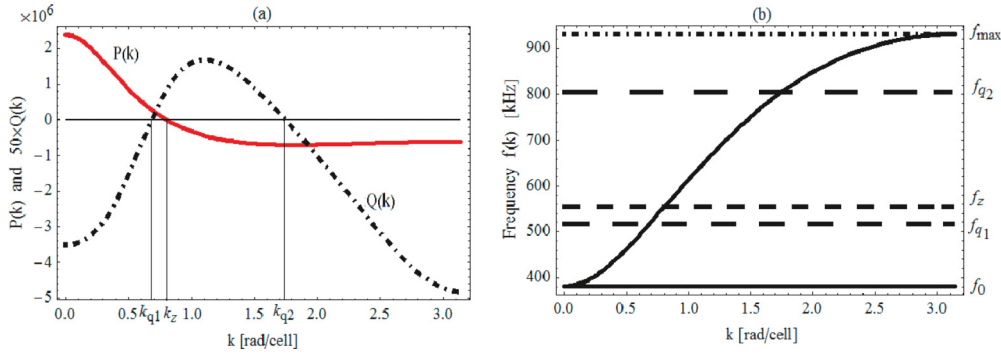


FIG. 2. (a) Behavior of the dispersive coefficient P (solid line) and plots of the nonlinear coefficient Q (dotted-dashed line) as functions of the wave number k for network parameters (2). (b) Linear dispersive curve showing the evolution of the frequency $f = \omega/2\pi$ as a function of the wave number k for network parameters (2). Here, $f_z = \omega(k_z)/2\pi$, $f_{q_1} = \omega(k_{q_1})/2\pi$, and $f_{q_2} = \omega(k_{q_2})/2\pi$, with k_z and k_{q_1} and k_{q_2} being respectively the zeros of $P(k)$ and $Q(k)$.

number k . With the help of Fig. 2(a), we have divided, as one can see from Fig. 2(b), the frequency domain $[f_0, f_{\max}]$ into four regions concerning the modulational instability of the plane wave and the possible soliton solutions of the GP Eq. (7a): two regions of positive PQ ($]f_{q_1}, f_z[$ and $]f_{q_2}, f_{\max}[$) corresponding to the MI of the plane wave and leading to envelope solitons, and two regions of negative PQ ($]f_0, f_{q_1}[$ and $]f_z, f_{q_2}[$) corresponding to the modulational stability of the plane wave and leading to hole solitons.

III. ANALYTICAL INVESTIGATION OF SOLITON PROPAGATION IN THE NETWORK OF FIG. 1

With the help of the solitary wave solutions of the GP Eq. (7a), we investigate in this section the propagation of both bright ($PQ > 0$) and dark ($PQ < 0$) solitary waves in the network of Fig. 1. To experience the propagation of solitary waves through the model shown in Fig. 1 for several bands of frequencies, we follow Marquie *et al.* [26] and excite the left extremity of the network with a solitary wave solution of the GP Eq. (7a). To avoid signal reflection that disturbs the accurate observation of the wave propagation in the line, the voltage across the right extremity is set to zero.

A. Propagation of bright solitary voltage signal in the network of Fig. 1

The propagation of bright solitary waves in the network of Fig. 1 is associated with the positivity of product PQ . As we have shown in the previous section, Eq. (7a) admits the continuous-wave solution

$$\psi_c(x, \tau) = A_c \exp[i\Delta_c(x, \tau)], \quad (12a)$$

$$\Delta_c(x, \tau) = K_c(\tau)x + A_c^2 Q\tau - P\omega_c(\tau) + \delta_{0c}, \quad (12b)$$

$$\frac{dK_c}{d\tau} = \lambda(\tau), \quad \frac{d\omega_c}{d\tau} = K_c^2(\tau).$$

Using the cw solution (12a) and (12b) as a seed solution, we follow Kengne and Talla [27] and look for bright solitonic wave solutions of Eq. (7a) in the form

$$\psi(x, \tau) = [A_c + \Phi(x, \tau)] \exp[i\Delta_c(x, \tau)], \quad (13)$$

where $\Phi(x, \tau)$ is a complex function. Inserting Eq. (13) into Eq. (7a) yields

$$i \frac{\partial \Phi}{\partial \tau} + P \frac{\partial^2 \Phi}{\partial x^2} + Q |\Phi|^2 \Phi + 2iPK_c \frac{\partial \Phi}{\partial x} + QA_c^2(\Phi + \Phi^*) + QA_c(\Phi^2 + 2|\Phi|^2) = 0. \quad (14)$$

Now, we seek solitary wave solutions of Eq. (14) in the form

$$\Phi(x, \tau) = A_s \frac{\gamma \cosh \xi + \cos \varphi + i\mu \sin \varphi}{\cosh \xi + \gamma \cos \varphi}, \quad (15)$$

where A_s , γ , and μ are three real constants with $\mu \neq 0$, and $\xi = \xi(x, \tau)$ and $\varphi = \varphi(\tau)$ are two real functions to be determined. Asking that function (15) satisfies Eq. (14), we obtain for $A_s \neq 0$, after some long calculations,

$$\xi(x, \tau) = A_s \mu \sqrt{\frac{Q}{2P}} [x - 2P\nu(\tau) + \tilde{\xi}_0],$$

$$\varphi(\tau) = A_s^2 \mu \frac{Q}{2P} \tau + \eta_0,$$

$$\mu^2 = \frac{A_s^2 - 4A_c^2}{A_s^2}, \quad \gamma = -\frac{2A_c}{A_s}, \quad \frac{d\nu}{d\tau} = K_c(\tau), \quad (16)$$

under the condition $A_s^2 - 4A_c^2 > 0$. Inserting Eq. (15) into Eq. (13), we obtain the following bright solitonic solution of Eq. (7a),

$$\psi(x, \tau) = \left(A_c + A_s \frac{\gamma \cosh \xi + \cos \varphi + i\mu \sin \varphi}{\cosh \xi + \gamma \cos \varphi} \right) \times \exp[i\Delta_c(x, \tau)]. \quad (17)$$

where ξ , φ , γ , and μ are defined by Eq. (16). Inserting solution (17) into Eq. (3) [we remember that $\chi_1(\tau) = 0$ so that $\psi(x, \tau) = u(x, \tau)$] and using Eqs. (6a) and (6b), we can analytically instigate the propagation of bright solitary waves in the network of Fig. 1.

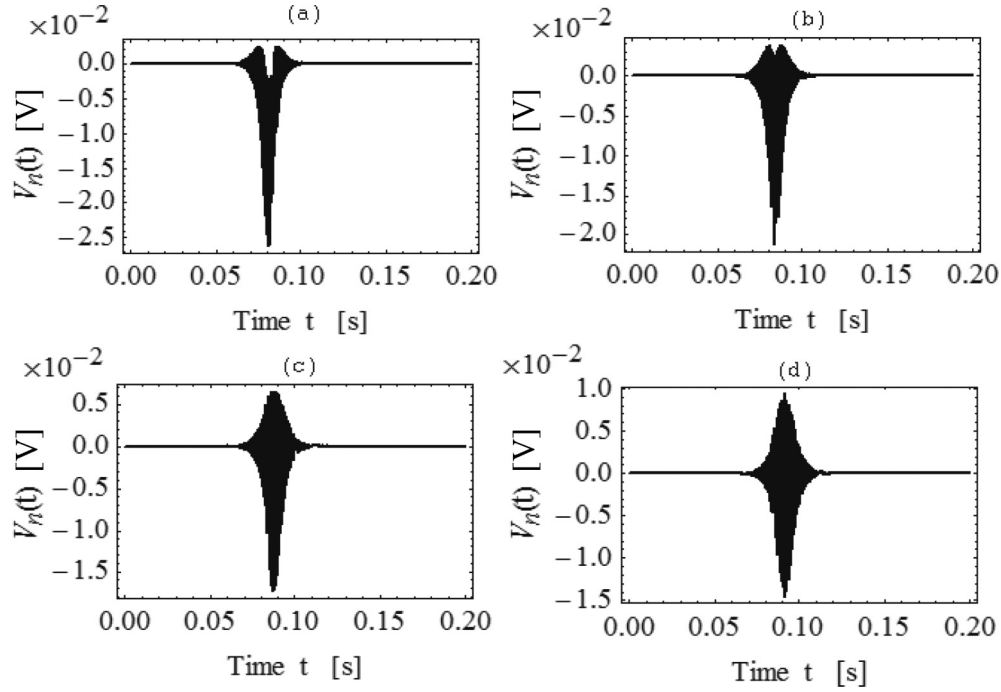


FIG. 3. Propagation of bright solitary signals [associated with solution (20) of the GP Eq. (7a)] at different frequencies through cell $n = 250$ of the network of Fig. 1 for solution parameters $\lambda_0 = 0.2$, $\nu_0 = 10^{-5}$, $K_0 = -100$, $\tilde{\delta}_{0c} = 0$, and $A_s = 6$. Solitary wave propagating at frequency (a) $f = 930.524$ kHz, (b) $f = 930.56$ kHz, (c) $f = 930.589$ kHz and (d) frequency $f = 930.61$ kHz. Different plots are obtained with the use of network parameters (2) and $\varepsilon = 10^{-3}$.

In solution (17) with parameters (16), A_c , A_s , $\tilde{\xi}_0$, and η_0 are arbitrary real constants. The constants $\tilde{\xi}_0$ and η_0 have the trivial effect of shifting the solutions in the x and t coordinates, respectively. Therefore, from now on we set $\tilde{\xi}_0 = \eta_0 = 0$. In what follows, we focus on two cases, $A_c A_s = 0$ and $A_c A_s \neq 0$.

1. Case $A_c A_s = 0$ and $|A_c| + |A_s| \neq 0$

When A_s vanishes or A_c vanishes, Eq. (17) turns into the cw background,

$$\psi(x, \tau) = A_c \exp[i\Delta_c(x, \tau)], \quad (18a)$$

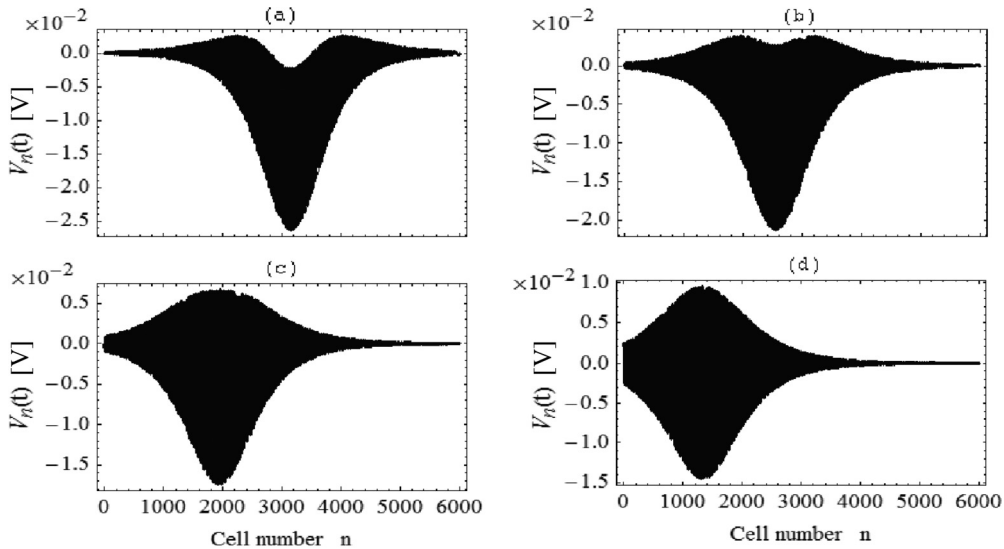


FIG. 4. Profile of bright solitary signals [associated with solution (20) of the GP Eq. (7a)] at time $t = 0.1$ s propagating at different frequencies for the network parameters (2) with $\varepsilon = 10^{-3}$ and solution parameters $\lambda_0 = 0.2$, $\nu_0 = 10^{-5}$, $K_0 = -100$, $\tilde{\delta}_{0c} = 0$, and $A_s = 6$. Solitary wave propagating at frequency (a) $f = 930.524$ kHz, (b) $f = 930.56$ kHz, (c) $f = 930.589$ kHz, and (d) $f = 930.61$ kHz.

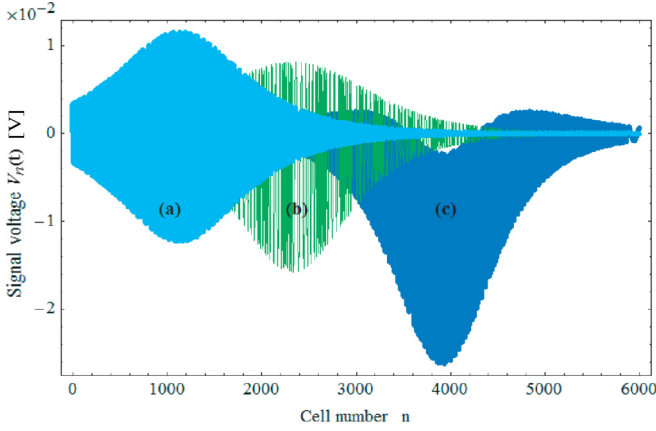


FIG. 5. Bright solitary signal voltage (in V) as a function of cell number n of the network at times $t = 0.105$ s of the propagation of a wave moving with different group velocities. Bright solitary wave moving with (a) group velocity $v_g = 4993.44$ cell/ms at carrier frequency $f = 930.626$ kHz, (b) group velocity $v_g = 16\,355.4$ cell/ms at carrier frequency $f = 930.6$ kHz, and (c) group velocity $v_g = 31\,507.9$ cell/ms at carrier frequency $f = 930.524$ kHz. To generate different plots, we have used the same network and solution parameters as in Figs. 3 and 4.

and into the bright soliton,

$$\psi(x, \tau) = \frac{A_s}{\cosh\left[A_s \sqrt{\frac{Q}{2P}} [x - 2Pv(\tau)]\right]} \times \exp[i\Delta_c(x, \tau) \pm i\varphi], \quad (18b)$$

respectively, where the analytical expression for $v(\tau)$ can be obtained by combining Eqs. (12b) and (16),

$$v(\tau) = \int_0^\tau \left[\int_0^y \lambda(z) dz + K_0 \right] dy + v_0, \quad (18c)$$

with $v_0 = v(0)$ and $K_0 = K_c(0)$ being two arbitrary real constants. Therefore, in general, the exact solution (17) describes a solitary wave embedded on a cw background [28], and when $A_c \ll A_s$, the background is small within the existence of the bright soliton. It is seen from solution (18b)

that (i) A_s is the amplitude of the bright soliton, and (ii) the center of the bright soliton is $\zeta(\tau) = 2Pv(\tau)$ and satisfies the equation

$$\frac{d^2\zeta}{d\tau^2} + 2\kappa(\tau)\zeta = 0, \quad (19)$$

with $\kappa(\tau) = -\frac{\lambda(\tau)}{2v(\tau)}$. Equation (19) means that the center of mass of the wave packet behaves as a classical particle, and allows one to manipulate the motion of bright solitons in the network by controlling the potential parameter $\lambda(\tau)$. (iii) The trajectory of a given soliton peak is obtained from the condition $\xi = 0$, leading to $x = 2Pv(\tau)$. In what follows, we take some examples to demonstrate the dynamics of bright solitons in the network of Fig. 1 associated with different kinds of strength $\lambda(\tau)$.

First, we consider the time-independent linear potential with strength $\lambda(\tau) = \lambda_0$ [see Eq. (7b)] and obtain the bright soliton solution

$$\psi(x, \tau) = \frac{A_s}{\cosh\left[A_s \sqrt{\frac{Q}{2P}} \left(x - 2P\left\{\frac{\lambda_0}{2}\tau^2 + K_0\tau + v_0\right\}\right)\right]} \times \exp[i\Delta(x, \tau)], \quad (20)$$

where $\Delta(x, \tau) = [\lambda_0\tau + K_0]x - P\left[\frac{\lambda_0^2}{3}\tau^3 + \lambda_0 K_0\tau^2 + K_0^2\tau\right] + A_s^2 \frac{Q}{2P}\tau + \tilde{\delta}_{0c}$. In this situation, the trajectory of a given soliton peak is $x(\tau) = P\lambda_0\tau^2 + 2PK_0\tau + 2Pv_0$. The trajectory is thus parabolic in time with an acceleration of $d^2x/d\tau^2 = 2P\lambda_0$. Mathematically, the trajectory of a given soliton peak will be concave left on (the curve is situated at the left of the tangent at each of its points) if $P\lambda_0 > 0$ and concave right on (the curve is situated at the right of the tangent at each of its points) if $P\lambda_0 < 0$.

With the use of solution (20) of the GP Eq. (7a), we show respectively in Figs. 3 and 4 the time evolution of solitary signals at different frequencies through cell $n = 250$ of the network of Fig. 1 and the solitary wave profiles at time $t = 0.1$ s propagating at different frequencies. As we can see from these plots, the form of a solitary wave along both the time and space axes depends on its frequency. Waves shown in plots (a)–(d) of

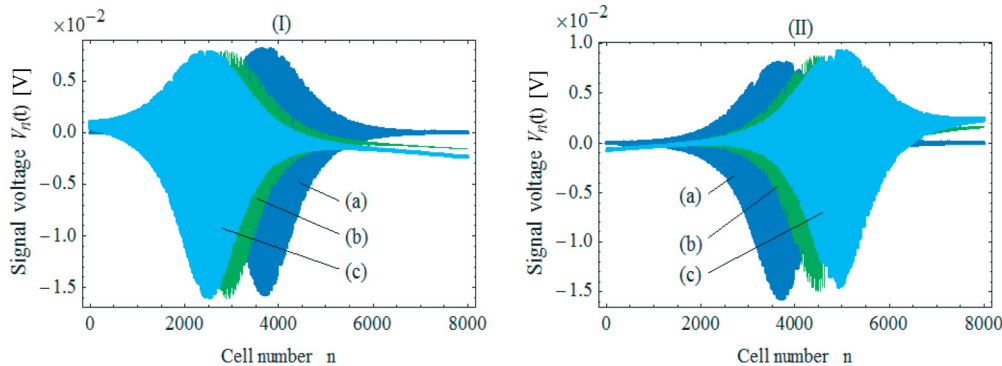


FIG. 6. Effects of strength $\lambda(\tau)$ of the linear trapping potential on a bright solitary signal voltage propagating at a frequency $f = 930.6$ kHz through the network of Fig. 1. Plots of the left panel (I) show the profiles of a bright solitary signal voltage at time $t = 0.115$ s for (a) $\lambda_0 = 0.2$, (b) $\lambda_0 = 10^8$, and (c) $\lambda_0 = 1.5 \times 10^8$, while plots of the right panel (II) show the profiles of a bright solitary signal voltage at time $t = 0.115$ s for (a) $\lambda_0 = -0.2$, (b) $\lambda_0 = -10^8$, and (c) $\lambda_0 = -1.5 \times 10^8$. To generate different plots, we have used the same network and solution parameters as in Fig. 3.

Figs. 3 and 4 propagate with group velocities $v_g = 31\,507.9$, $25\,446.3$, $19\,385.5$, and $13\,325.4$ cell/ms, respectively. The plots of Figs. 3 and 4 also show that the wave speed increases with the group velocity of the propagating wave. This behavior is well seen in Fig. 5. Figures 3–5 also reveal that the bright solitary voltage oscillates symmetrically around the zero voltage as the carrier frequency approaches the cutoff frequency $f_{\max} = 930.628$ kHz. Figure 6 shows the profiles at time $t = 0.115$ s of bright solitary signal voltages obtained for different strengths $\lambda(\tau) = \lambda_0$ of the linear trapping potential. The plots of this figure reveal that (i) the bright solitary wave velocity decreases as strength $\lambda(\tau) = \lambda_0 > 0$ increases and $\lambda(\tau) = \lambda_0 < 0$ decreases, and (ii) the bright solitary wave oscillates symmetrically around the zero voltage for only small λ_0 . This last behavior is well seen in Fig. 6(d). The plots of Fig. 6 thus

show how much strength $\lambda(\tau) = \lambda_0$ of the linear trapping potential may affect the wave trajectory and its velocity. It is important to note that all carrier frequencies f used in Figs. 3–6 are taken in the MI region satisfying the conditions $P(k) < 0$ and $Q(k) < 0$ (the rightmost region in Fig. 2). Therefore, $P\lambda_0 > 0$ for negative λ_0 and $P\lambda_0 < 0$ for positive λ_0 .

Second, we consider the temporal periodic modulation of the linear potential with strength $\lambda(\tau) = \lambda_0(1 + m \sin a\tau)$, where $\lambda_0 \neq 0$ and $a \neq 0$ are any real numbers, and $0 < m < 1$. According to Eqs. (12b) and (18c), we have $K_c(\tau) = \lambda_0(\tau - \frac{m}{a} \cos a\tau) + K_0$, $v(\tau) = \lambda_0(\frac{1}{2}\tau^2 - \frac{m}{a^2} \sin a\tau) + K_0\tau + v_0$, and $\omega_c(\tau) = \frac{\lambda_0^2}{3}\tau^3 + K_0\lambda_0\tau^2 + (K_0^2 + \frac{\lambda_0^2 m^2}{2a^2})\tau - (\frac{2K_0\lambda_0 m}{a^2} + \frac{2m\lambda_0^2}{a^2}\tau) \sin a\tau - \frac{2m\lambda_0^2}{a^3} \cos a\tau + \frac{m^2\lambda_0^2}{4a^3} \sin 2a\tau + \omega_{c0}$. According to Eq. (18b), we get the bright one-solitary wave

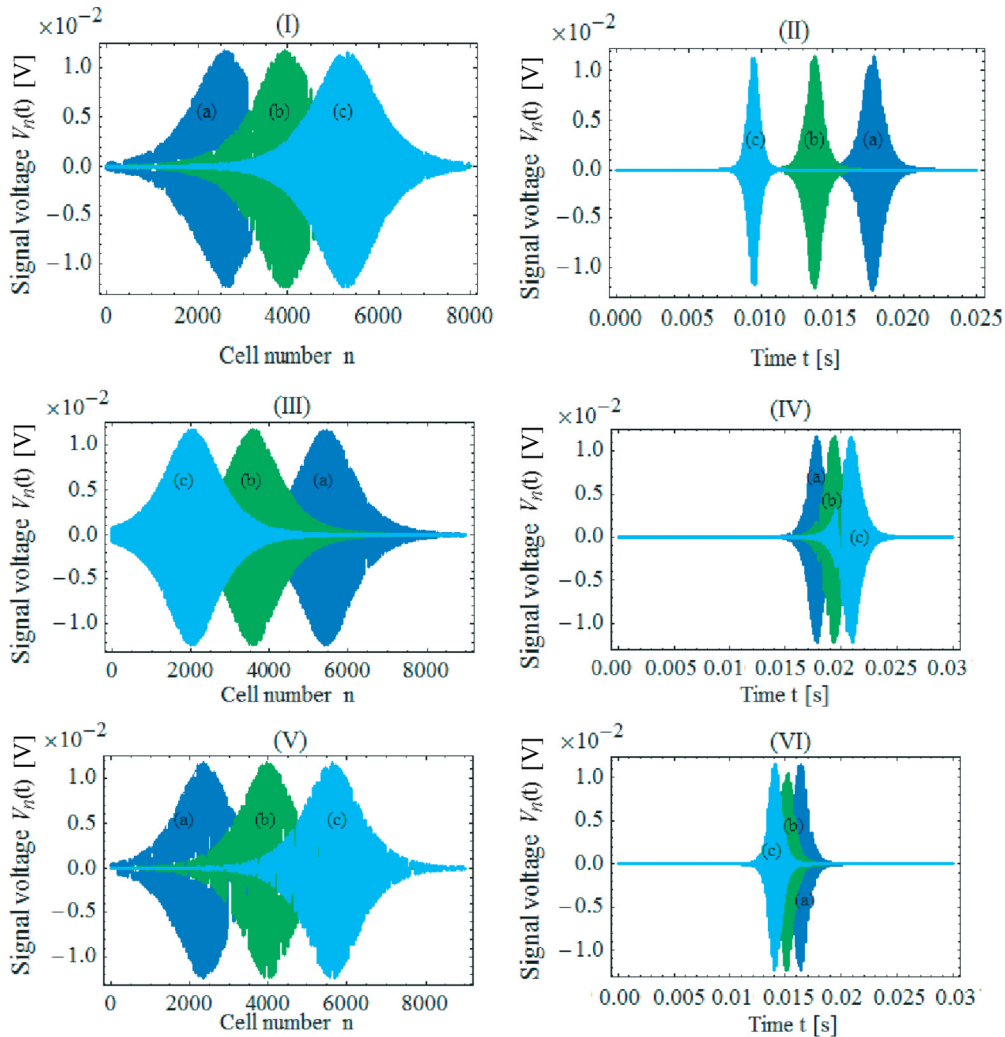


FIG. 7. Effects of the strength $\lambda(\tau)$ on bright solitary waves propagating at a carrier frequency $f = 930.626$ kHz for the network parameters (2) with $\varepsilon = 10^{-3}$ and for the solution parameters [see Eq. (21)] $v_0 = 15 \times 10^{-6}$, $K_0 = -100$, $\tilde{\delta}_0 = \omega_{c0} = 0$. The top plots (I) and (II) respectively show the spatial evolution at time $t = 0.022$ s and the temporal evolution through cell $n = 250$ of a bright solitary signal voltage in the network for $m = 0.1$, $a = 0.2$, and three values of parameter λ_0 : (a) $\lambda_0 = 1350$, (b) $\lambda_0 = 1450$, and (c) $\lambda_0 = 1550$. The middle plots (III) and (IV) respectively show the spatial evolution at time $t = 0.025$ s and the temporal evolution through cell $n = 250$ of a bright solitary signal voltage in the network for $\lambda_0 = 1500$, $m = 0.1$, and three values of parameter a : (a) $a = 0.2$, (b) $a = 0.22$, and (c) $a = 0.24$. The bottom plots (V) and (VI) respectively show the spatial evolution at time $t = 0.2$ s and the temporal evolution through cell $n = 250$ of a bright solitary signal voltage in the network for $\lambda_0 = 1500$, $a = 0.2$, and three values of parameter m : (a) $m = 0.11$, (b) $m = 0.12$, and (c) $m = 0.13$.

solution

$$\psi(x, \tau) = \frac{A_s}{\cosh \left[A_s \sqrt{\frac{Q}{2P}} \left(x - 2P \left\{ \frac{\lambda_0}{2} \tau^2 + K_0 \tau - \frac{\lambda_0 m}{a^2} \sin a \tau + \nu_0 \right\} \right) \right]} \exp [i \Delta(x, \tau)], \quad (21)$$

where $\Delta(x, \tau) = K_c(\tau)x + A_s^2 \frac{Q}{2P} \tau - P\omega_c(\tau) + \tilde{\delta}_0$. In the present situation, the trajectory of a given soliton peak is $x(\tau) = P\lambda_0 \tau^2 + 2PK_0 \tau - \frac{2P\lambda_0 m}{a^2} \sin a \tau + \nu_0$.

With the use of solution (21), we show in Fig. 7, for different parameters of the strength $\lambda(\tau)$, the spatial (left panels) and temporal (right panel) evolution of the bright solitary signal voltage. The top, middle, and bottom plots are obtained with different values of λ_0 , a , and m , respectively. Plot (I) shows that the bright solitary wave oscillates symmetrically around the zero voltage with a velocity that increases with λ_0 , while plot (II) reveals that the lifetime of a bright solitary signal through a given cell increases as the parameter λ_0 decreases. Comparing the top and middle plots, we conclude that λ_0 and

a have opposite effects on the propagation of bright solitary waves through the network. It is seen from the top and bottom plots that parameters λ_0 and m have the same effect as the wave propagation; indeed, when parameter a is chosen such that $\sin a \tau$ remains positive, the strength $\lambda(\tau)$ of the trapping potential increases with each λ_0 and m .

2. Case $A_c A_s \neq 0$

Here, we investigate the situation when solution (17) with parameters (16) describes solitary waves embedded on continuous-wave backgrounds. Let us rewrite solution (17) here,

$$\psi(x, \tau) = \left(A_c + A_s \frac{-2A_c \cosh \xi + A_s \cos \varphi \pm i \sqrt{A_s^2 - 4A_c^2} \sin \varphi}{A_s \cosh \xi - 2A_c \cos \varphi} \right) \exp [i \Delta_c(x, \tau)], \quad (22a)$$

$$\xi(x, \tau) = A_s \sqrt{\frac{Q(A_s^2 - 4A_c^2)}{2PA_s^2}} [x - 2P\nu(\tau)], \quad \varphi(\tau) = A_s \sqrt{A_s^2 - 4A_c^2} \frac{Q}{2P} \tau. \quad (22b)$$

An analysis of Eqs. (22a) and (22b) reveals that the velocity for the solitary wave still satisfies Eq. (19). In particular, when $\lambda(\tau) = \lambda_0 \exp [a\tau]$ with real parameters λ_0 and a satisfying the condition $\lambda_0 a \neq 0$, we find $\nu(\tau) = \frac{\lambda_0}{a^2} \exp [a\tau] + K_{c0} \tau + \nu_0$ and $\Delta_c(x, \tau) = \left(\frac{\lambda_0}{a} \exp [a\tau] + K_{c0} \right) x + (QA_c^2 - PK_{c0}^2) \tau - P \left(\frac{2K_{c0}\lambda_0}{a^2} \exp [a\tau] + \frac{\lambda_0^2}{2a^3} \exp [2a\tau] \right) + \Delta_{c0}$, with K_{c0} , ν_0 , and Δ_{c0} being three arbitrary real constants. For the network parameters (2), $\varepsilon = 10^{-2}$, for solution parameters $\Delta_{c0} = \omega_{c0} = 0$, $K_{c0} = 2 \times 10^{-5}$, $\nu_0 = 0$, $A_s = 1$, and for the strength $\lambda = 570 \exp [-12t]$ (that is, $\lambda_0 = 570$ and $a = -12$), we show in Fig. 8, for different values of A_c , the propagation of bright solitary voltage signals embedded on continuous-wave backgrounds. In Figs. 8(a) and 8(b), $A_c = 10^{-3} \ll 1 = A_s$ and the background is neglected (invisible) within the

existence of the bright solitary wave. In Figs. 8(c) and 8(d), $A_c = 0.1 = A_s/10$ and the background is small (but visible) within the existence of the bright solitary wave. In Figs. 8(e) and 8(f), $A_c = 0.499 \simeq A_s/2$ and the background is large within the existence of the bright solitary wave.

B. Propagation of dark solitary voltage signal in the network of Fig. 1

Now, we consider the case when $PQ < 0$, leading to a dark soliton solution of the GP Eq. (7a). In this case, we seek a dark soliton solution of Eq. (7a) in the form $\psi_d(x, \tau) = (A_c + iA_s \tanh [y(x, \tau)]) \exp [iK_d(\tau)x + i\Lambda_d(\tau)]$, where $y(x, \tau) = \rho_0 x + y_0(\tau)$, $K_d(\tau)$, and $\Lambda_d(\tau)$ are functions to be determined, and ρ_0 , ρ_c , and ρ_s are three real parameters. Asking that $\psi_d(x, \tau)$ satisfies Eq. (7a) leads to

$$\psi_d(x, \tau) = \sqrt{-\frac{2P}{Q}} \left(\rho_c \pm i\rho_s \tanh \left[\rho_s \left(x \pm \sqrt{-\frac{Q}{2P}} y_0(t) \right) \right] \right) \exp [iK_d(\tau)x + i\Lambda_d(\tau)], \quad (23)$$

$$\frac{dK_d}{d\tau} = \lambda(\tau), \quad (24)$$

$$\frac{d\Lambda_d}{d\tau} = -2P(\rho_c^2 - \rho_s^2) - PK_d^2, \quad (25)$$

$$\frac{dy_0}{d\tau} = -2P \sqrt{-\frac{Q}{2P}} (\rho_c \pm K_d), \quad (26)$$

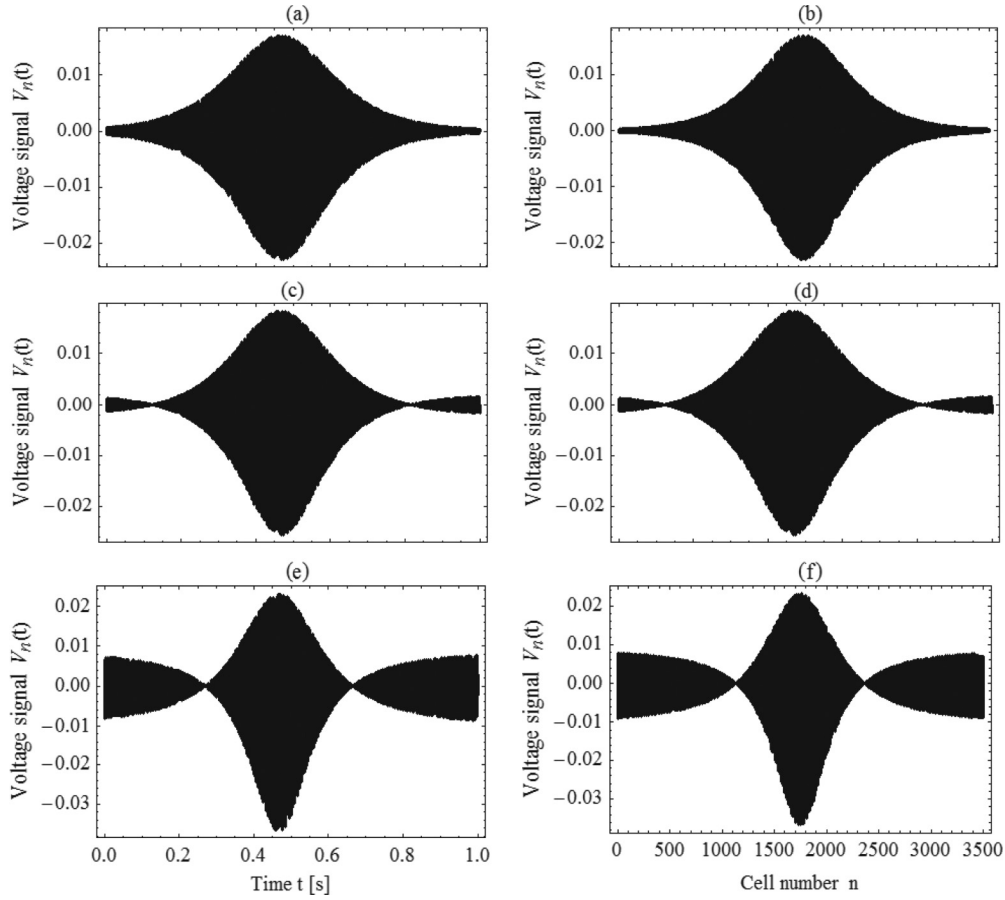


FIG. 8. Propagation at frequency $f = 930.62$ kHz of bright solitary voltage signals associated with the solitary wave embedded on a continuous-wave background (22a) and (22b) for different values of the solution parameter A_c : (a), (b) $A_c = 10^{-3}$; (c), (d) $A_c = 0.1$; (e), (f) $A_c = 0.499$. The left plots show the evolution of solitary bright signals embedded on continuous-wave backgrounds through cell $n = 600$. The right plots show the spatial profile at time $t = 0.1$ s of solitary bright signals embedded on continuous-wave backgrounds in the network. Different parameters used to generate these plots are given in the text.

where $\rho_s = A_s \sqrt{-\frac{Q}{2P}}$ and $\rho_c = A_c \sqrt{-\frac{Q}{2P}}$. When $\rho_s = 0$ or $\rho_c = 0$, $\psi_d(x, \tau)$ reduces respectively to the background $\psi_d(x, \tau) = \rho_c \sqrt{-\frac{2P}{Q}} \exp[iK_d(\tau)x + i\Lambda_d(\tau)]$ and the dark solitary wave $\psi_d(x, \tau) = \pm i\rho_s \sqrt{-\frac{2P}{Q}} \tanh[\rho_s(x \pm \sqrt{-\frac{2P}{Q}}y_0(t))] \exp[iK_d(\tau)x + i\Lambda_d(\tau)]$. Thus, $\psi_d(x, \tau)$ represents a dark solitary wave embedded in the background. It is seen from Eq. (23) that the amplitude of the dark soliton is proportional to $\sqrt{-2P/Q}$, while the width is inversely proportional to $\sqrt{-2P/Q}$. Thus Eq. (23) can be used to describe the compression of dark solitary waves when $\sqrt{-Q/2P}$ increases with the wave number k . Because of the relationships between $\lambda(\tau)$ and K_d [see Eq. (24)], the soliton speed $v_d(\tau) = dx/d\tau = \mp Q(\rho_c \pm K_d)$ is intimately dependent on the potential parameter $\lambda(\tau)$. In our numerical simulation, we focus on the case with the “+” sign in Eqs. (23) and (26).

Inserting solution (23) into Eq. (3) [we remember that $\chi_1(\tau) = 0$ so that $\psi(x, \tau) = u(x, \tau)$] and using Eqs. (6a) and (6b), we can analytically instigate the evolution of a dark solitary voltage signal in the network of Fig. 1 when the wave frequencies are taken from the region

of modulational stability of the plane wave, i.e., when product PQ is negative. In the special case of a time-independent linear trap potential, that is, when $\lambda(\tau) = \lambda_0$ is a nonzero constant, Eqs. (24)–(26) lead to $K_d(\tau) = \lambda_0\tau + K_{d0}$, $\Lambda_d(\tau) = -2P(\rho_c^2 - \rho_s^2)\tau - \frac{P}{3\lambda_0}(\lambda_0\tau + K_{d0})^3 + \Lambda_{d0}$, and $y_0(\tau) = -2P\sqrt{-\frac{Q}{2P}}(\rho_c\tau + \frac{1}{2\lambda_0}(\lambda_0\tau + K_{d0})^2) + y_{00}$, where K_{d0} , Λ_{d0} , and y_{00} are three arbitrary real constants. In this situation, the soliton speed is $v_d(\tau) = -Q\lambda_0\tau - Q(\rho_c + K_{d0})$. Depending on the size and the sign of the potential parameter λ_0 , the soliton speed $v_d(\tau)$ can either be positive during its propagation or negative during its propagation.

The main parameters appearing in solution (23)–(26) in the special case $\lambda(\tau) = \lambda_0 \neq 0$ are the wave amplitudes ρ_c and ρ_s , the wave numbers $k = k_p$ leading to the propagating frequencies $f = f_p = \omega(k_p)/2\pi$, and the potential parameter λ_0 . Other free parameters K_{d0} , Λ_{d0} , and y_{00} appear when integrating Eqs. (24)–(26). Figures 9–11 show the time evolutions of a dark solitary voltage signal through cell $n = 350$ of the network for respectively different A_c and A_s , different wave numbers k , and different values of parameters λ . As it is seen from these figures, each main parameter ρ_c , ρ_s , k , and λ_0 leads to a particular profile of a dark solitary wave propagating through the network. Each of these three figures

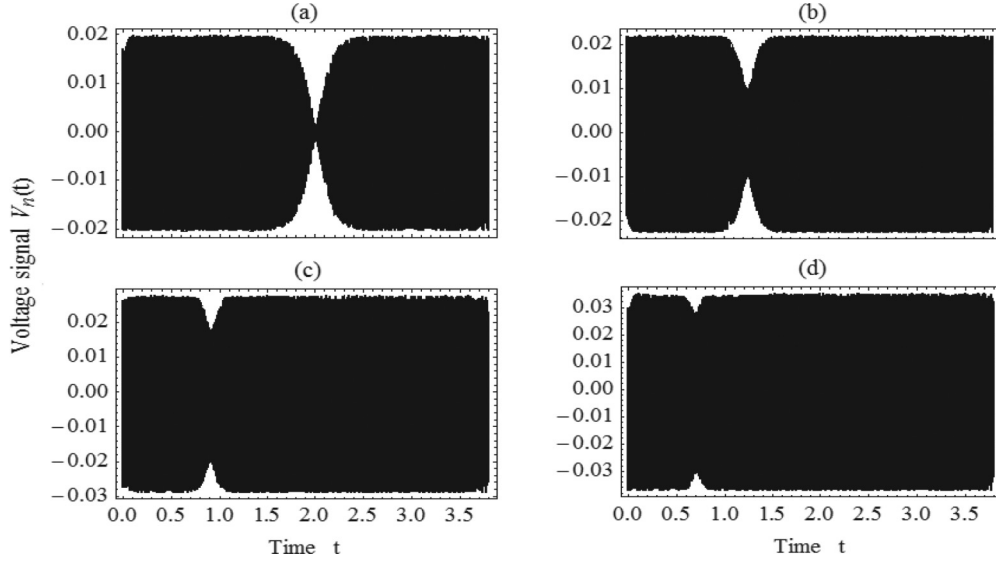


FIG. 9. Effects of the continuous-wave background on a dark solitary voltage signal propagating through cell $n = 350$ at frequency $f = f_p = 381.655$ kHz for $\rho_s = 0.12139$, $\lambda_0 = 0.1$, $y_{00} = 11.2$, $K_{d0} = 10^{-5}$, $\Lambda_{d0} = 0$, and (a) $\rho_c = 0$, (b) $\rho_c = 0.0606949$, (c) $\rho_c = 0.12139$, and (d) $\rho_c = 0.182085$.

is obtained with the use of the network parameters (2) and $\varepsilon = 10^{-2}$. Figure 9 shows the effects of the continuous-wave background on a dark solitary wave. Figure 9(a) shows a dark solitary wave propagating on a vanishing continuous-wave background, i.e., when $\rho_c = 0$. Figures 9(b)–9(d) show dark solitary waves embedded on a continuous-wave background with respectively $\rho_c < \rho_s$, $\rho_c = \rho_s$, and $\rho_c > \rho_s$. The plots of Fig. 9 show that the depth of the dark soliton decreases as the parameter ρ_c of the background increases. It is seen from Figs. 9(a)–9(d) that when $\rho_c \ll \rho_s$ or $\rho_s \ll \rho_c$, the background is small within the existence of a dark soliton or the dark soliton is small within the existence of a continuous-wave background. Figure 10 shows how much the carrier frequency $f = f_p$

impacts the behavior of dark solitary waves embedded on continuous-wave backgrounds during its propagation through a given cell of the network. The change in the behavior (deformation) of the wave with its carrier frequency is due to the coefficient of u^2 in the expression of the second-harmonic terms ψ_2 given by Eq. (6b). The effects of the potential parameter $\lambda = \lambda_0$ on dark solitons embedded on continuous-wave backgrounds are shown in Fig. 11, showing the time evolution of the dark solitary voltage signal for positive (top plots) and negative (bottom plots) values of the parameter λ_0 . The top and bottom plots show that the velocity of the dark soliton decreases when the potential parameter λ_0 increases.

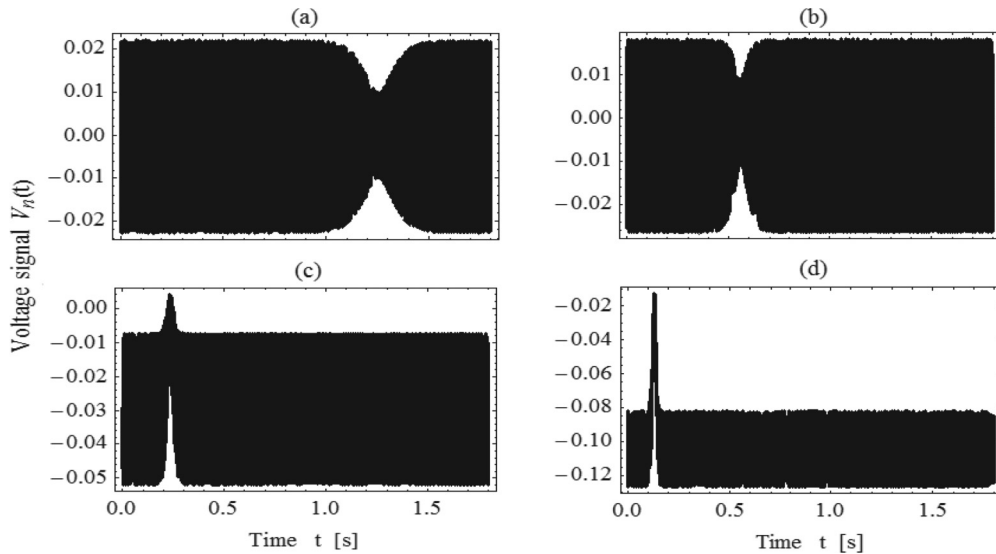


FIG. 10. Influence of the carrier frequency on wave behavior during its propagation through cell $n = 350$ of the network for $\rho_s \sqrt{-\frac{2P}{Q}} = 1$, $\rho_c \sqrt{-\frac{2P}{Q}} = 0.5$, $\lambda_0 = 0.1$, $y_{00} = 11.2$, $K_{d0} = 10^{-5}$, $\Lambda_{d0} = 0$. (a) Time evolution of a dark soliton embedded on a continuous-wave background for the frequency $f = f_p = 381.655$ kHz, (b) $f = f_p = 381.658$ kHz, (c) $f = f_p = 381.679$ kHz, and (d) $f = f_p = 381.74$ kHz.

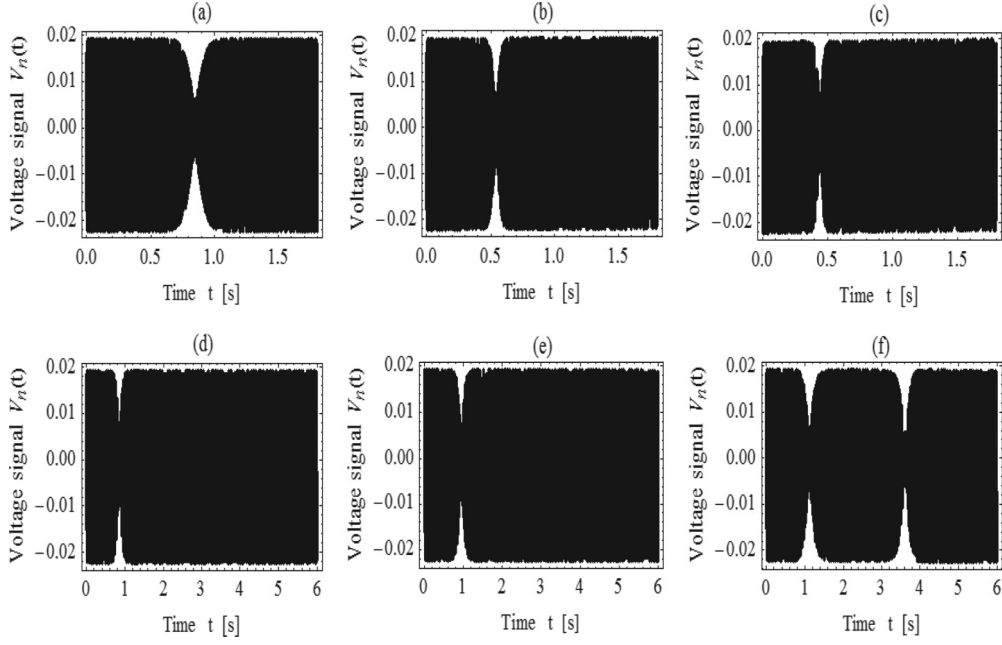


FIG. 11. Effects of the linear trap potential parameter $\lambda = \lambda_0$ on dark solitary waves propagating at a frequency $f = f_p = 381.656$ kHz through cell $n = 350$ of the network for $\rho_s = 0.12139$, $\rho_c = 0.036417$, $y_{00} = 11.2$, $K_{d0} = 10^{-5}$, $\Lambda_{d0} = 0$. The top plots show the time evolution of dark soliton for positive λ_0 : (a) $\lambda_0 = 10$, (b) $\lambda_0 = 5000$, and (c) $\lambda_0 = 10^4$. The bottom plots show the time evolution of a dark soliton for positive λ_0 : (d) $\lambda_0 = -10$, (e) $\lambda_0 = -500$, and (f) $\lambda_0 = -10^3$.

One of the features of Fig. 11 is that the behavior of the dark soliton shown in Fig. 11(f) is different from that of other waves [Figs. 11(a)–11(e)]. Does Fig. 11(f) show an interaction of two dark solitons embedded on the same continuous-wave background? Our numerical computations have shown that the wave behavior in Fig. 11(f) occurs for many other $\lambda_0 \in [\lambda_{01}, \lambda_{02}]$, where $\lambda_{01} < -100 < \lambda_{02}$. As we can see from Fig. 12, the behavior shown in Fig. 11(f) also depends on ρ_c .

C. Experimental validation

Suppose we have a pulse generator, for example, a programmable generator that allows us to create highly custom pulse shapes by varying the amplitude at various points. Moreover, suppose we have a numerical oscilloscope XSC1 which has a high impedance that is used to avoid signal reflection. Then, for the experimental validation of our results, one can follow Marquie *et al.* [26] and consider a nonlinear electrical network with $N = 45$ identical cells in which each

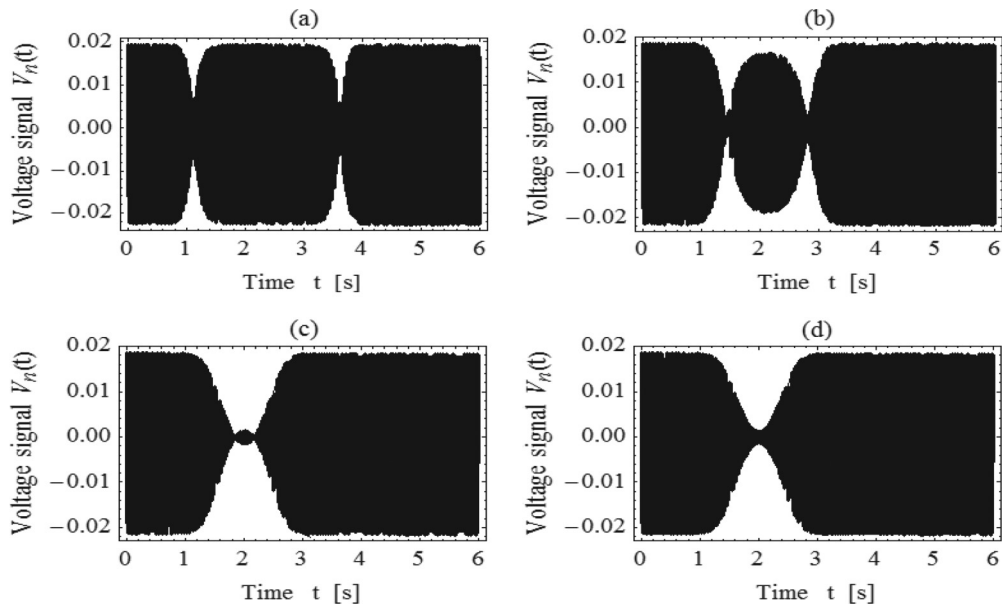


FIG. 12. Impacts of the continuous-wave background on the behavior of dark solitary voltage signals propagating through cell $n = 350$ at frequency $f = f_p = 381.656$ kHz for $\rho_s = 0.12139$, $\lambda_0 = -10^3$, $y_{00} = 11.2$, $K_{d0} = 10^{-5}$, $\Lambda_{d0} = 0$, and (a) $\rho_c = 0.036417$, (b) $\rho_c = 0.012139$, (c) $\rho_c = 0.0012139$, and (d) $\rho_c = 0$.

diode BB112 is biased by $V_b = 2$ V, and matched by a resistor in order to simulate an infinite line. The waves are then created by using the programmable generator, and the wave forms are observed and stored by using the numerical oscilloscope XSC1. After finding the best shape for unaltered propagation (soliton), this could be compared to our theoretical results.

IV. CONCLUSION

In this paper, we have considered a modified Noguchi electrical network and, by applying the reductive perturbation method in the semidiscrete limit, we have showed that the dynamics of the modulated waves in the network can be governed by a Gross-Pitaevskii equation with a time-dependent linear potential in the presence of a chemical potential. We have shown that the potential parameter does not affect the growth rate (gain) of the MI of our system.

We have found exact analytical solitary wave solutions of the GP equation with derived time-dependent linear potentials for both cases of modulational instability and modulational stability of our system. Using these exact analytical solutions, we have investigated numerically the transmission of both bright and dark solitary voltage signals in the network, and the effects of the potential parameter as well as those of the carrier frequency on the propagation of solitary voltage waves embedded on cw backgrounds in the network. Our studies showed that the behavior of solitary waves propagating in the network simultaneously depend on the wave frequency, on the potential parameter, and on the amplitude of the cw background. Our exact analytical solitary wave solutions can be useful for investigating the dynamics of modulated waves in other physical systems described by a GP equation with a time-dependent linear potential, such as one-dimensional Bose-Einstein condensates.

-
- [1] A. C. Scott, *Nonlinear Science: Emergence and Dynamics of Coherent Structures* (Oxford University Press, New York, 1999).
 - [2] A. Hasegawa, *Optical Solitons in Fibers*, 2nd ed. (Springer, Berlin, 1989).
 - [3] M. Remoissenet, *Waves Called Solitons*, 3rd ed. (Springer, Berlin, 1999).
 - [4] N. J. Zabusky and M. D. Kruskal, *Phys. Rev. Lett.* **15**, 240 (1965).
 - [5] K. Lonngren, in *Solitons in Action*, edited by K. Lonngren and A. Scott (Academic, New York, 1978).
 - [6] T. Taniuti and N. Yajima, *J. Math. Phys.* **10**, 1369 (1969).
 - [7] F. I. Ndzana, A. Mohamadou, T. C. Kofané, and L. Q. English, *Phys. Rev. E* **78**, 016606 (2008).
 - [8] F. B. Pelap, J. H. Kamga, S. B. Yamgoue, S. M. Ngounou, and J. E. Ndecfo, *Phys. Rev. E* **91**, 022925 (2015).
 - [9] E. Kengne, V. Bozic, M. Viana, and R. Vaillancourt, *Phys. Rev. E* **78**, 026603 (2008).
 - [10] T. Kakutani and N. Yamasaki, *J. Phys. Soc. Jpn.* **45**, 674 (1978).
 - [11] A. C. Newell and J. V. Moloney, *Nonlinear Optics* (Addison-Wesley, Boston, 1991).
 - [12] F. S. Yamasaki, L. P. S. Neto, J. O. Rossi, and J. J. Barroso, *IEEE Trans. Plasma Sci.* **42**, 3471 (2014).
 - [13] R. Hirota and K. Suzuki, *Proc. IEEE* **61**, 1483 (1973).
 - [14] A. C. Scott, *Active and Nonlinear Wave Propagation in Electronics* (Wiley-Interscience, New York, 1970).
 - [15] R. Marquié, J. M. Bilbault, and M. Remoissenet, *Physica D* **87**, 371 (1995).
 - [16] H. Malwe Boudoue, B. Gambo, S. Y. Dokab, and T. Crepin Kofane, *Appl. Math. Comput.* **239**, 299 (2014).
 - [17] E. Afshari and A. Hajimiri, *IEEE J. Solid-State Circ.* **40**, 744 (2005).
 - [18] E. Kengne and W. M. Liu, *Phys. Rev. E* **73**, 026603 (2006).
 - [19] D. Yemélé and F. Kenmogné, *Phys. Lett. A* **373**, 3801 (2009).
 - [20] D. Ndjanfang, D. Yemélé, P. Marquié, and T. C. Kofané, *Prog. Electromagn. Res. B* **52**, 207 (2013).
 - [21] X. Oriols and F. Martín, *J. Appl. Phys.* **90**, 2595 (2001).
 - [22] E. Kengne, A. Lakhssassi, and W. M. Liu, *Phys. Rev. E* **91**, 062915 (2015).
 - [23] M. Remoissenet, *Waves Called Solitons*, 2nd ed. (Springer, Berlin, 1996).
 - [24] E. Lundh, C. J. Pethick, and H. Smith, *Phys. Rev. A* **55**, 2126 (1997).
 - [25] U. Al Khawaja, C. J. Pethick, and H. Smith, *Phys. Rev. A* **60**, 1507 (1999).
 - [26] P. Marquié, J. M. Bilbault, and M. Remoissenet, *Phys. Rev. E* **49**, 828 (1994).
 - [27] E. Kengne and P. K. Talla, *J. Phys. B: At. Mol. Opt. Phys.* **39**, 3679 (2006).
 - [28] L. Wu, J.-F. Zhang, and L. Li, *New J. Phys.* **9**, 69 (2007).